JOC Article

Novel Pyromellitic Diimide-Based Macrocycle with a Linear π-Electronic System and Bis(phenylethynyl)pyromellitic Diimide: Syntheses, Structures, Photophysical Properties, and Redox Characteristics[1]

Shin-ichiro Kato,[†,‡] Yasuhiro Nonaka,[†,‡] Toshiaki Shimasaki,[†,‡] Kenta Goto,[†] and Teruo Shinmyozu*[,†]

Institute for Materials Chemistry and Engineering (IMCE) and Department of Molecular Chemistry, Graduate School of Sciences, Kyushu University, Hakozaki 6-10-1 Higashi-ku, Fukuoka 812-8581, Japan

shinmyo@ms.ifoc.kyushu-u.ac.jp

Received February 13, 2008

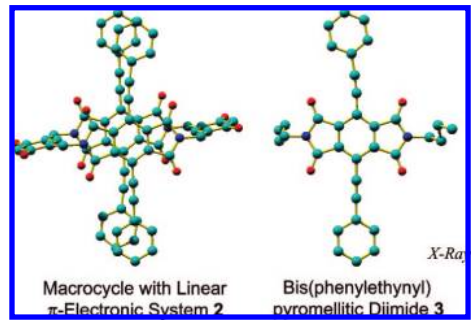

We report the syntheses, structures, photophysical properties, and redox characteristics of the [2 + 2] pyromellitic diimide-based macrocycle with a linear π-electronic system **2** as well as the 3,6-bis(phenylethynyl)pyromellitic diimide derivative **3**. The interesting solid state structural properties of the clathrates of **3** with π-donors are also reported. The macrocycle **2** was synthesized by the direct cyclocondensation followed by the Sonogashira coupling reaction. X-ray crystallographic studies showed that the phenylacetylene moieties in **2** formed the intramolecular benzene dimer structures, and the bis(phenylethynyl)pyromellitic diimide moieties in both **2** and **3** were stacked in a parallel and slanted arrangement. Theoretical calculations for **2′** and **3** suggested the existence of electrostatic interactions between the bis(phenylethynyl)pyromellitic diimide moieties. The UV/vis spectral measurements and TDDFT calculations of **2**, **2′**, and/or **3** were performed to understand their electronic transitions. The fluorescence spectral measurements showed that **2** and **3** have visible fluorescence properties and **2** displays an excimer fluorescence at ca. 590 nm. The cyclic voltammetry measurements revealed that the electrostatic repulsion between the diimide moieties in **2** is greater than that in **1** according to the extension of the π-electronic systems. X-ray crystallography of the clathrates of **3** with various π-donors demonstrated the formation of the segregated donor−acceptor structures, indicating the strong aggregation ability of the bis(phenylethynyl)pyromellitic diimide moiety.

1. Introduction

Aromatic diimides, particularly naphthalene diimides (NDIs) and perylene bisimides (PBIs), are important compounds for material and supramolecular chemistry. In the past years, functionalized NDIs and PBIs[2] were tailored for applications in various research fields. Aromatic diimides are easily reversibly reduced to form stable radical anion species. Due to their n-type semiconducting properties, functionalized NDIs and PBIs

* To whom correspondence should be addressed. Phone: +81-92-642-2720. Fax: +81-92-642-2735.
† Institute for Materials Chemistry and Engineering.
‡ Department of Molecular Chemistry, Graduate School of Sciences, Kyushu University.

(1) Molecular Tubes and Capsules, Part 4. For Part 1−3, see refs 17a−c.

(2) (a) Würthner, F. *Chem. Commun.* **2004**, 1564–1579. (b) Grimsdale, A. C.; Müllen, K. *Angew. Chem., Int. Ed.* **2005**, *44*, 5592–5629. (c) Wasielewski, M. R. *J. Org. Chem.* **2006**, *71*, 5051–5066. (d) Würthner, F. *Pure Appl. Chem.* **2006**, *78*, 2341–2350.

10.1021/jo800283r CCC: $40.75 © 2008 American Chemical Society
Published on Web 04/23/2008

have been of much interest as the active layer in organic field-effect transistors (OFETs).[3,4] In this context, the preparation of core-substituted naphthalene dianhydrides as versatile precursors has been most recently explored to develop the NDI-based future functional materials by Würthner et al.[5] In supramolecular chemistry, aromatic diimides with both an electron-withdrawing property and extended π-surface, which exploit the charge-transfer (CT) interactions between aromatic π-systems, i.e., alkoxynaphthalenes, have been used in the design of a plethora of supramolecular architectures, such as [2]catenanes,[6,7] [2]rotaxanes,[8] folded aedamers,[9] and macrocycle-tweezer complexes.[10] Additionally, the aggregation of PBIs with solubilizing 3,4,5-trialkoxyphenyl and 3,4,5-trialkylphenyl substituents at the imide functional groups were achieved both in solution and in the condensed phase on the basis of their strong π-stacking interactions and van der Waals interactions.[11] Afterward, it was recently reported that NDIs and PBIs, which enable π-stacking interactions, hydrogen bonding, and van der Waals interactions, formed robust 1D organogel structures.[12] Thus, the created supramolecular structures could be regarded as candidates for the attractive functional materials due to the presence of photophysically and electrochemically active aromatic diimides.[13]

Pyromellitic diimides, which have only a central benzene core, are the smallest moieties among the class of aromatic diimides. Pyromellitic diimides also have a sufficient electron affinity and can interact with electron-rich π-systems by CT interactions in solution and the solid state regardless of the smallness of their core π surfaces relative to NDIs and PBIs. Therefore, the creation of supramolecular architectures,[14] especially [2]catenanes[7a–f] and [2]rotaxanes,[8b–d] and their applications to molecular receptors[15] have been achieved due to their peculiar properties similar to those of the NDIs and PBIs. Although the functionalized pyromellitic diimides would be important compounds in terms of their optoelectronic and electrochemical properties, only a limited number of them have been reported.[16]

We have been investigating the molecular recognition properties of pyromellitic diimide-based macrocycles, which were synthesized by the cyclocondensation of commercially available pyromellitic dianhydride and alkoxy-substituted bis(aminomethyl)arenes.[17] Recently, we reported the first example of "cyclophanes within cyclophanes" based on CT interactions as the driving force, which has been confirmed by X-ray crystallography.[17a] Furthermore, we have more recently synthesized the macrocycle **1**, and **1** constructs 1D and 2D supramolecular assemblies with naphthols in the solid states with the regioselectivity of the hydroxyl groups of the naphthols and exhibits redox modulations via noncovalent interactions with the naphthols (Figure 1).[17b] As a part of our continuing effort to develop this type of pyromellitic diimide-based macrocycle, we planned to synthesize a macrocycle with a linear π-electronic system **2** and bis(phenylethynyl)pyromellitic diimide **3** in which the phenylethynyl groups were introduced at the core benzene rings because of the interest in the effect of the elongated π-system in the pyromellitic diimide moiety on their optoelectronic and electrochemical properties (Figure 1). Compounds **2** and **3** are regarded as aromatic acetylene analogues which are now recognized as ideal materials for advanced applications.[18,19] We now report the synthesis of **2** and **3** and their electronic

(3) (a) Katz, H. E.; Lovinger, A. J.; Johnson, J.; Kloc, C.; Siegrist, T.; Li, W.; Lin, Y.-Y.; Dodabalapur, A. *Nature* **2000**, *404*, 478–481. (b) Katz, H. E.; Johnson, J.; Lovinger, A. J.; Li, W. *J. Am. Chem. Soc.* **2000**, *122*, 7787–7792. (c) Hizu, K.; Sekitani, T.; Someya, T.; Otsuki, J. *Appl. Phys. Lett.* **2007**, *90*, 093504.

(4) (a) Jones, B. A.; Ahrens, M. J.; Yoon, M.-H.; Facchetti, A.; Marks, T. J.; Wasielewski, M. R. *Angew. Chem., Int. Ed.* **2004**, *43*, 6363–6366. (b) Chesterfield, R. J.; Mckeen, J. C.; Newman, C. R.; Ewbank, P. C.; da Silva Filho, D. A.; Brédas, J.-L.; Miller, L. L.; Mann, K. R.; Frisbie, C. D. *J. Phys. Chem. B* **2004**, *108*, 19281–19292. (c) Jung, T.; Yoo, B.; Wang, L.; Dodabalapur, A.; Jones, B. A.; Facchetti, A.; Wasielewski, M. R.; Marks, T. J *Appl. Phys. Lett.* **2006**, *88*, 183012(13). (d) Yoo, B.; Madgavkar, A.; Jones, B. A.; Nadkarni, S.; Facchetti, A.; Dimmler, K.; Wasielewski, M. R.; Marks, T. J.; Dodabalapur, A. *IEEE Electron Device Lett.* **2006**, *27*, 737–739. (e) Wang, Y.; Chen, Y.; Li, R.; Wang, S.; Su, W.; Ma, P.; Wasielewski, M. R.; Jiang, J. *Langmuir* **2007**, *23*, 5842–5863.

(5) (a) Thalacker, C.; Röger, C.; Würthner, F. *J. Org. Chem.* **2006**, *71*, 8098–8105. (b) Röger, C.; Würthner, F. *J. Org. Chem.* **2007**, *72*, 8070–8075.

(6) For a review of catenanes and oligocatenanes, see: Raehm, L.; Hamilton, D. G.; Sanders, J. K. M. *Synlett* **2002**, 1743–1761.

(7) For [2]catenanes, see: (a) Hamilton, D. G.; Sanders, J. K. M.; Davies, J. E.; Clegg, W.; Teat, S. J. *Chem. Commun.* **1997**, 897–898. (b) Hamilton, D. G.; Davies, J. E.; Prodi, L.; Sanders, J. K. M. *Chem. Eur. J.* **1998**, *4*, 608–620. (c) Hamilton, D. G.; Feeder, N.; Prodi, L.; Teat, S. J.; Clegg, W.; Sanders, J. K. M. *J. Am. Chem. Soc.* **1998**, *120*, 1096–1097. (d) Zhang, Q.; Hamilton, D. G.; Feeder, N.; Teat, S. J.; Goodman, J. M.; Sanders, J. K. M. *New J. Chem.* **1999**, *23*, 897–903. (e) Hamilton, D. G.; Prodi, L.; Feeder, N.; Sanders, J. K. M. *J. Chem. Soc., Perkin Trans. 1* **1999**, 1057–1065. (f) Hamilton, D. G.; Montalti, M.; Prodi, L.; Fontani, M.; Zanello, P.; Sanders, J. K. M. *Chem. Eur. J.* **2000**, *6*, 608–617. (g) Hansen, J. G.; Feeder, N.; Hamilton, D. G.; Gunter, M. J.; Becher, J.; Sanders, J. K. M. *Org. Lett.* **2000**, *2*, 449–452. (h) Gunter, M. J.; Farquhar, S. M. *Org. Biomol. Chem.* **2003**, *1*, 3450–3457. (i) Fallon, G. D.; Lee, M. A.-P.; Langford, S. J.; Nichols, P. J. *Org. Lett.* **2004**, *6*, 655–658. (j) Kaiser, G.; Jarrosson, T.; Otto, S.; Ng, Y.-F.; Bond, A. D.; Sanders, J. K. M. *Angew. Chem., Int. Ed.* **2004**, *43*, 1959–1962.

(8) For [2]rotaxanes, see: (a) Nakamura, Y.; Minami, S.; Iizuka, K.; Nishimura, J. *Angew. Chem., Int. Ed.* **2003**, *42*, 3158–3162. (b) Wang, X-Z.; Li, X.-Q.; Shao, X.-B.; Zhao, X.; Deng, P.; Jiang, X.-K.; Li, Z.-T.; Chen, Y.-Q. *Chem. Eur. J.* **2003**, *9*, 2904–2913. (c) Vignon, S. A.; Jarrosson, T.; Iijima, T.; Tseng, H.-R.; Sanders, J. K. M.; Stoddart, J. F *J. Am. Chem. Soc.* **2004**, *126*, 9884–9885. (d) Iijima, T.; Vignon, S. A.; Tseng, H.-R.; Jarrosson, T.; Sanders, J. K. M.; Marchioni, F.; Venturi, M.; Apostoli, E.; Balzani, V.; Stoddart, J. F. *Chem. Eur. J.* **2004**, *10*, 6375–6392.

(9) (a) Lokey, R. S.; Iverson, B. L. *Nature* **1995**, *375*, 303–305. (b) Nguyen, B. L.; Iverson, B. L. *J. Am. Chem. Soc.* **1999**, *121*, 2639–2640. (c) Gabriel, G. J.; Iverson, B. L. *J. Am. Chem. Soc.* **2002**, *124*, 15174–15175.

(10) (a) Colquhoun, H. M.; Zhu, Z.; Williams, D. J. *Org. Lett.* **2003**, *5*, 4353–4356. (b) Colquhoun, H. M.; Zhu, Z. *Angew. Chem., Int. Ed.* **2004**, *43*, 5040–5045.

(11) (a) Würthner, F.; Thalacker, C.; Diele, S.; Tschierske, C. *Chem. Eur. J.* **2001**, *7*, 2245–2253. (b) Würthner, F.; Chen, Z.; Dehm, V.; Stepanenko, V. *Chem. Commun.* **2006**, 1188–1190.

(12) (a) Li, X.-Q.; Stepanenko, V.; Chen, Z.; Prins, P.; Siebbeles, L. D. A.; Würthner, F. *Chem. Commun.* **2006**, 3871–3873. (b) Mukhopadhyay, P.; Iwashita, Y.; Shirakawa, M.; Kawano, S.; Fujita, N.; Shinkai, S. *Angew. Chem., Int. Ed.* **2006**, *45*, 1592–1595.

(13) For the recent examples, see: (a) Chen, Z.; Stepanenko, V.; Dehm, V.; Prins, P.; Siebbeles, L. D. A.; Seibt, J.; Marquetand, P.; Engel, V.; Würthner, F. *Chem. Eur. J.* **2007**, *13*, 436–449. (b) Chen, Z.; Baumeister, U.; Tschierske, C.; Würthner, F. *Chem. Eur. J.* **2007**, *13*, 450–465.

(14) For pyromellitic diimide-bassed molecular duplexes, see: (a) Zhou, Q.-Z.; Jiang, X.-K.; Shao, X.-B.; Chen, G.-J.; Jia, M.-X.; Li, Z.-T. *Org. Lett.* **2003**, *5*, 1955–1958. (b) Zhou, Q.-Z.; Jia, M.-X.; Shao, X.-B.; Wu, L.-Z.; Jiang, X.-K.; Li, Z.-T.; Chen, G.-J. *Tetrahedron* **2005**, *61*, 7117–7124.

(15) (a) Chen, G.; Lean, J. T.; Alcalá, M.; Mallouk, T. E. *J. Org. Chem.* **2001**, *66*, 3027–3034. (b) Colquhoun, H. M.; Williams, D. J.; Zhu, Z. *J. Am. Chem. Soc.* **2002**, *124*, 13346–13347.

(16) Fox et al. have most recently reported the synthesis of π-conjugated compounds based on pyromellitic diimide moiety, *N*,*N*′-di(2-*tert*-butylphenyl)-3,6-di(4-chlorophneyl)pyromellitic diimide, by the approach different from ours. See: Dong, Z.; Liu, X.; Yap, G. P. A.; Fox, J. M. *J. Org. Chem.* **2007**, *72*, 617–625.

(17) (a) Iwanaga, T.; Yasutake, M.; Takemura, H.; Sako, K.; Shinmyozu, T. *Angew. Chem., Int. Ed.* **2006**, *45*, 3643–3647. (b) Kato, S.; Matsumoto, T.; Ideta, K.; Shimasaki, T.; Goto, K.; Shinmyozu, T. *J. Org. Chem.* **2006**, *71*, 4723–4733. (c) Kato, S.; Nakagaki, T.; Shimasaki, T.; Shinmyozu, T. *CrystEngComm* In press.

(18) (a) Stang, P. J.; Diederich, F., Eds. *Modern Acetylene Chemistry*; Wiley-VCH: Weinheim, 1995. (b) de Meijere, A., Ed. *Top. Curr. Chem. (Carbon Rich Compounds I)*; Springer: Berlin, Germany, 1998; Vol. 196. (c) de Meijere, A., Ed. *Top. Curr. Chem. (Carbon Rich Compounds I)*; Springer: Berlin, Germany, 1999; Vol. 201. (d) Diederich, F.; Stang, P. J.; Tykwinski, R. R., Eds. *Acetylene Chemistry: Chemistry, Biology, and Material Science*; Wiley-VCH: Weinheim, Germany, 2005. (e) Haley, M. M.; Tykwinski, R. R., Eds. *Carbon-Rich Compounds: From Molecules to Materials*; Wiley-VCH: Weinheim, Germany, 2006.

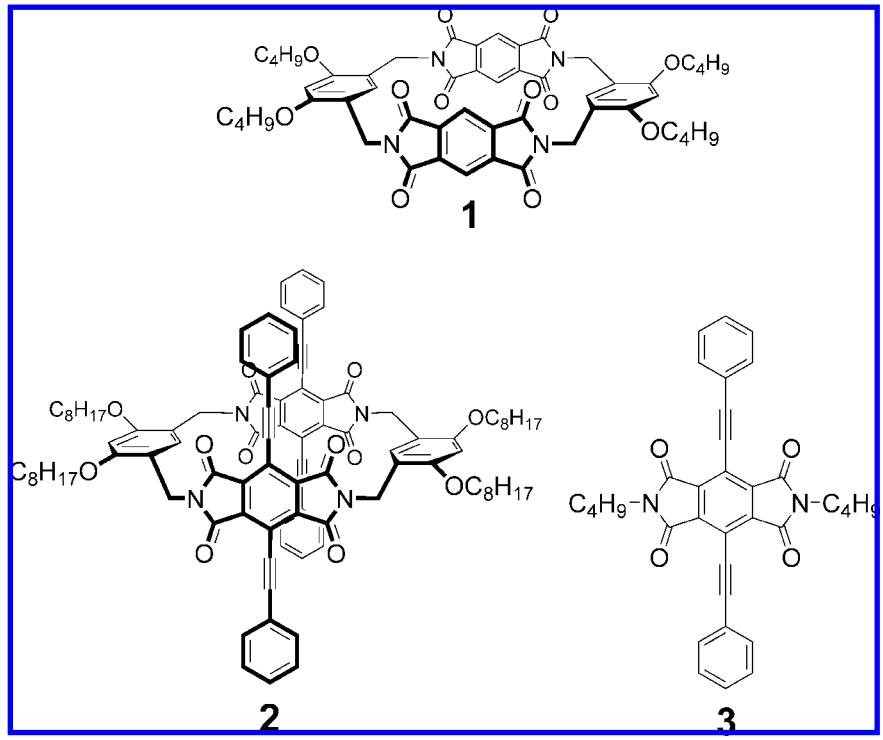

FIGURE 1. Structures of the [2 + 2] pyromellitic diimide-based macrocycle **1**, macrocycle with a linear π-electronic system **2**, and bis(phenylethynyl)pyromellitic diimide **3**.

properties, based on their electronic and fluorescence spectra, and redox potentials. The structures of **2** and **3** and the unusual aggregation ability of the bis(phenylethynyl)pyromellitic diimide moiety in the solid state are also discussed on the basis of the X-ray crystallographic analyses, theoretical calculations, and MALDI-TOF mass spectrum. Finally, the formation of the CT complexes and segregated donor−acceptor crystal structures of **3** with various π-donors are demonstrated in UV/vis titration studies and X-ray crystallography results, respectively.

2. Results and Discussion

Synthesis. The synthesis of the [2 + 2] pyromellitic diimide-based macrocycle with a linear π-electronic system **2** was achieved by cyclocondensation followed by Sonogashira coupling as the key reactions (Scheme 1). The solubilizing octyloxy groups were engineered into **2** to alleviate the anticipated solubility problems. 1,3-Bis(aminomethyl)-4,6-dioctyloxy-benzene (**8**) was prepared from resorcinol (**4**) by a similar series of reactions reported for the preparation of 1,3-bis(aminomethyl)-4,6-di-*n*-butoxybenzene.[17b,20] 1,3-Di-*n*-octyloxybenzene (**5**)[21]was transformed into the diiode **6** by ICl at room temperature (92%). The cyanation of **6** with CuCN in NMP afforded the dinitrile **7** (59%), which was converted into the diamine **8** by reduction with DIBAL-H at 110 °C (53%). The cyclocondensation of **8** and 3,6-dibromopyromellitic dianhydride (**9**), which was prepared from durene in 3 steps,[22,23] followed by dehydration with NaOAc and Ac_2O gave the [2 + 2] tetrabromo-substituted macrocycle **10** (12%). The ^{1}H NMR spectrum of the macrocycle **10** is very simple, exhibiting a pair of two singlets at 6.49 and 6.52 ppm in $CDCl_3$ due to the spacer benzene protons in line with its D_{2h}-symmetric structure. Although the solubility of the macrocycle **10** in organic solvents was very poor, it was purified by silica gel column chromatography ($CHCl_3$/hexane) because the higher oligomers, such as [3 + 3] and [4 + 4] macrocycles, were not isolated. Finally, the Sonogashira coupling reaction[24] of **10** with phenylacetylene in the presence of $PdCl_2(PPh_3)_2$ as a catalyst afforded the desired **2** (23%).[25] For the comparison of the photophysical and electrochemical properties of the macrocycle **2**, the acyclic reference compound, *N*,*N*′-di-*n*-butyl-3,6-bis(phenylethynyl)pyromellitic diimide **3**, was prepared from the anhydride **9** by a similar procedure for the synthesis of **2**. Compounds **2** and **3** have been fully characterized by various

(19) For recent reviews of aromatic acetylenes, see: (a) Diederich, F.; Gobbi, L. *Top. Curr. Chem.* **1999**, *201*, 43–79. (b) Haley, M. M.; Pak, J. J.; Brand, S. C. *Top. Curr. Chem.* **1999**, *201*, 81–130. (c) Bunz, U. H. F.; Rubin, Y.; Tobe, Y. *Chem. Soc. Rev.* **1999**, 101–119. (d) Youngs, W. J.; Tessier, C. A.; Bradshaw, J. D. *Chem. Rev.* **1999**, *99*, 3153–3180. (e) Bunz, U. H. F. *Chem. Rev.* **2000**, *100*, 1605–1644. (f) Tour, J. M. *Acc. Chem. Res.* **2000**, *33*, 791–804. (g) Simsen, P.; Livingston, R. C.; Diederich, F. *Angew. Chem., Int. Ed.* **2000**, *39*, 2632–2657. (h) Diederich, F. *Chem. Commun.* **2001**, 219–227. (i) Zhao, D.; Moore, J. S. *Chem. Commun.* **2003**, 807–818. (j) Spitler, E. L.; Johnson, C. A.; Haley, M. M. *Chem. Rev.* **2006**, *106*, 5344–5386. (k) Orita, A.; Otera, J. *Chem. Rev.* **2006**, *106*, 5387–5412.

(20) Sasaki, S.; Mizuno, M.; Naemura, K.; Tobe, Y. *J. Org. Chem.* **2000**, *65*, 275–283.

(21) (a) Mohr, B.; Enkelmann, V.; Wegner, G. *J. Org. Chem.* **1994**, *59*, 635–638. (b) Higuchi, T.; Satake, C.; Hirobe, M. *J. Am. Chem. Soc.* **1995**, *117*, 8879–8880.

(22) Suh, D. H.; Chung, E. Y.; Hong, Y.-T; Choi, K.-Y. *Angew. Makromol. Chem.* **1998**, *254*, 33–38.

(23) To our knowledge, the detailed procedures of **9** have not been described in the literature.[22] Thus, our procedure was described in the Experimental Section. The use of unpurified **9** significantly decreased the cyclocondensation yield (less than 1%) probably due to the side reactions.

(24) (a) Sonogashira, K.; Tohda, Y.; Hagihara, N. *Tetrahedron Lett.* **1975**, *16*, 4467–4470. (b) Sonogashira, K. *J. Organomet. Chem.* **2002**, *653*, 46–49.

(25) We also prepared the tetrabromide **12** with the dibutoxy substituents at the benzene linkers (Experimental Section) by the cyclocondensation of the anhydride **9** and 1,3-bis(aminomethyl)-4,6-di-*n*-butoxybenzene and attempted the Sonogashira reaction of **12** with phenylacetylene under the same reaction conditions for the synthesis of **2**. However, the reaction resulted in the quantitative recovery of **12** due to the poor solubility of **12** in common organic solvents.

SCHEME 1. Synthesis of Pyromellitic Diimide-Based Macrocycle with Linear π-Electronic System 2 and Bis(phenylethynyl)-pyromellitic Diimide 3[a]

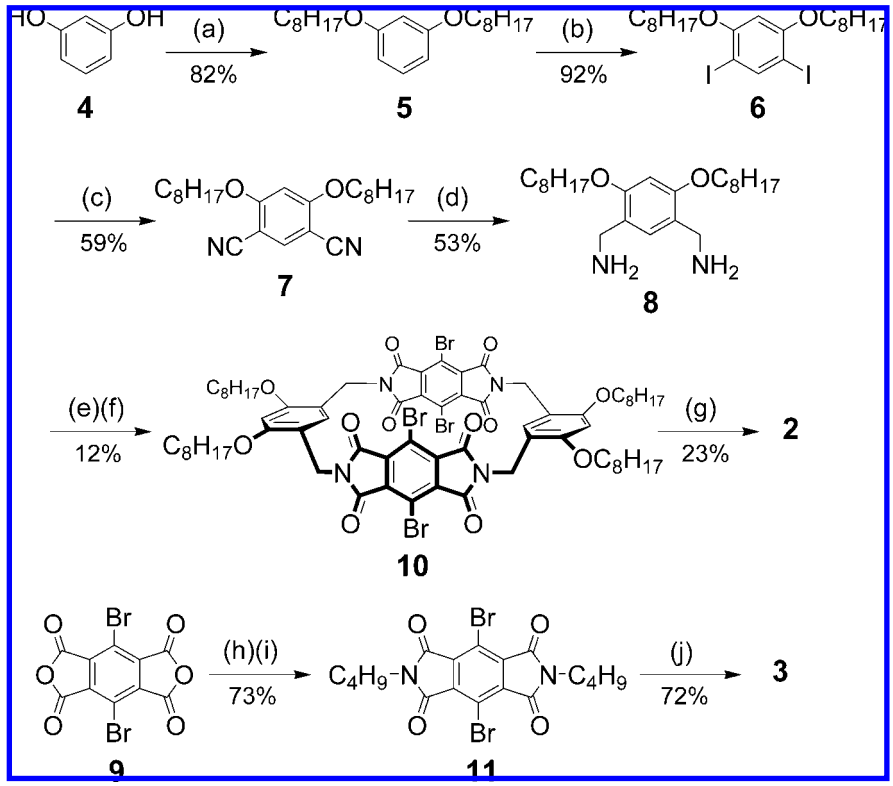

[a] Reagents and conditions: (a) 1-bromooctane, NaI, K_2CO_3, acetone, reflux for 48 h; (b) ICl, AcOH, rt for 3 h; (c) CuCN, NMP, 150 °C for 10 h; (d) DIBAL-H, toluene, 110 °C for 4 h; (e) compound **9**, THF, 50 °C for 24 h; (f) NaOAc, Ac_2O, rt for 3 h to 100 °C for 1 h; (g) phenylacetylene, $PdCl_2(PPh_3)_2$, CuI, Et_3N, THF, 75 °C for 36 h; (h) *n*-butylamine, rt for 12 h; (i) NaOAc, Ac_2O, 100 °C for 1 h; (j) phenylacetylene, $PdCl_2(PPh_3)_2$, CuI, Et_3N, THF, 75 °C for 12 h.

spectroscopic methods and elemental analysis,[26] and finally by X-ray crystallographic analyses as described below.

Structural Properties. Single crystals of **2** suitable for an X-ray crystallographic analysis were obtained by recrystallization from DMF. We reported that **1** formed a clathrate compound with DMF (**1**:DMF = 1:2),[17b] but DMF was not included in the single crystals of **2** (Figure 2). The transannular pyromellitic diimide moieties with phenylacetylene units of **2** were set in parallel (Figure 2a). The phenyl rings of the phenylacetylene units of **2** were slightly twisted against the benzene ring of the diimide moieties with the dihedral angles for C1−C10−C29−C30 and C4−C5−C21−C26 of −12.3° and 15.1°, respectively. The dihedral angle between the benzene ring of the diimide moiety and the benzene ring of the xylyl moiety was 80.6°. Interestingly, the phenyl rings of the phenylacetylene units were stacked in a parallel-displaced geometry with the distance between the centers of the two facing benzene rings of 3.39 Å and formed the benzene dimer (Figure 2b). The angle between the plane of the benzene ring and the stacking axis was 64.0°. The transannular distance (3.39 Å) of the benzene rings was almost equal to the sum of the van der Waals radii of the two sp^2 carbons (2 × 1.7 Å) or the value of the common stacked π-system (3.4 Å).[27] In the benzene dimer structure, the incline of the benzene ring of the phenylacetylene unit and the facing benzene ring was only 2.8°. The transannular distance between the benzene rings of the diimide moieties was only 4.09 Å, and this indicated a significant decrease (ca. 20%) in the distance compared to the corresponding distance of **1** (5.06 Å). It is well documented that the attractive interaction in the benzene dimer would increase in the perpendicular T-shaped and parallel-displaced geometries.[28] The observed benzene dimer geometry of **2** almost satisfied this geometrical requirement to maximize the attractive interactions, which can compensate for the destabilization caused by the deformation of the pyromellitic diimide moieties. However, the deformation of the pyromellitic diimide moieties of **2** was not observed in the optimized structure calculated at the B3LYP/6-31G* level of theory (Figure S30, Supporting Information).[29] Therefore, the crystal packing force also would contribute to the geometry of **2** observed in the X-ray crystallography spectrum.

Figure 3a shows the side view of the packing arrangement of **2**, and the molecules were packed in a parallel and slanted arrangement with the intermolecular distance between the center of the benzene ring of the pyromellitic diimide moiety and the

(26) Unfortunately, we could not carry out the variable-temperature ^1H NMR experiments for **2** and **10** due to their solubility problem in CD_2Cl_2. The macrocycle **2** easily crystallized below 0 °C and **10** did not dissolve in common organic solvents.

(27) The standard van der Waals radii are taken from: Bondi, A. *J. Phys. Chem.* **1964**, *68*, 441–451.

(28) For review of high-accuracy quantum mechanical studies in benzene dimers, see: Sinnokrot, M. O.; Sherrill, C. D. *J. Phys. Chem. A* **2006**, *110*, 10656–10668.

(29) In the optimized structure of **2′** at the B3LYP/6-31G* level, the transannular distance between the benzene rings of the diimide moieties is 5.17 Å: This value is clearly larger than the experimental value. It is pointed out that the underestimation of attractive $\pi-\pi$ interaction is common to anthracene−acetylene oligomers at the B3LYP/6-31G level by Toyota et al, see: Ishikawa, T.; Shimasaki, T.; Akashi, H.; Toyota, S. *Org. Lett.* **2008**, *10*, 417–420.

(30) The stacking in the parallel and slanted arrangement was not observed in **1**·(DMF) clathrate, where DMF served as an adhesive that bound the diimide molecules to form the 1D network.[17b]

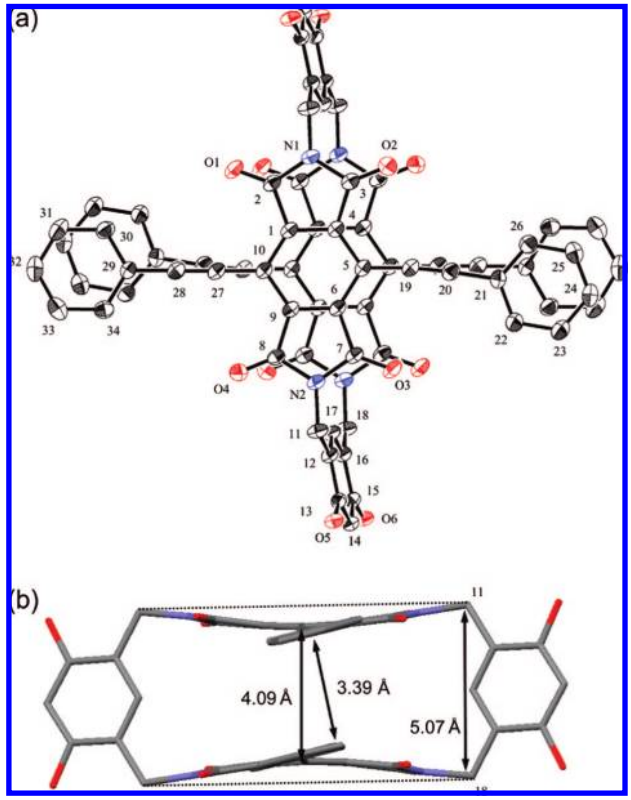

FIGURE 2. (a) ORTEP drawing of the top view of **2**. Thermal ellipsoids are drawn at the 50% probability level; (b) X-ray crystal structure of the side view of **2**. Hydrogen atoms and octyl groups of **2** are omitted for clarity.

plane of facing molecule of 3.25 Å and with an angle between the plane of the diimide and the stacking axis of 42.5°. This distance is shorter than the common distance between the stacked π-system (3.4 Å), strongly indicating the electronic interaction between these π-systems.[30] To examine the nature of the intermolecular interaction, the Mulliken charge was calculated for **2′**, in which the octyloxy groups were replaced with methoxy groups in **2**, by the DFT method (B3LYP/6-311G**//B3LYP/6-31G*).[31] As expected from the features of the carbonyl group, the carbonyl carbon atoms and oxygen atoms were found to be positive (+0.43) and negative (−0.30), respectively (Figure 3b). The adjacent sp^2 benzene carbon atom bearing an acetylene moiety was negatively charged (−0.20). The closest intermolecular distances were observed between the carbonyl carbon and the C-1 carbon atom of the benzene ring in the phenylacetylene unit as well as between the carbonyl carbon and oxygen atoms (Figure 3a). Thus, the electrostatic interactions might play an important role in the parallel and slanted packing of the molecules and provide that the intermolecular electrostatic repulsion between the diimide moieties was negligible.

Figure 3c shows the molecular packing of **2**. The macrocycle **2** packed by aligning in the *a*-axis in a parallel and slanted arrangement as described above. In addition, the intermolecular C−H···O interactions between the carbonyl oxygen atoms and the phenyl hydrogen atoms were observed as being aligned in the *b*-axis with an H···O distance of 2.67 (A of Figure 3c) and 2.42 (B of Figure 3c) Å, respectively.

Single crystals of **3** for an X-ray crystallographic analysis were obtained by recrystallization from *p*-xylene as a clathrate with *p*-xylene having a 2:1 stoichiometry. As shown in Figure 4b, the ORTEP drawing of **3** exhibited a nearly planar structure with the dihedral angles for C6−C9−C21−C26 and C7−C12−C29−C30 of −9.6° and 5.3°, respectively, and the trans conformation of the butyl groups on the nitrogen atoms.

The acyclic **3** also packed in a parallel and slanted arrangement as in the case of the macrocycle **2**, although two kinds of stacking arrangements were observed (Figure 5a).[32] The closest intermolecular distances between the center of the one diimide molecule and the π-face of another one of 3.21 ($\alpha-\beta$ of Figure 5a) and 3.23 ($\beta-\alpha$ of Figure 5a) Å were observed. The angle between the plane of the diimide molecule and the stacking axis was 42.5° ($\alpha-\beta$ of Figure 5a) and 43.0° ($\beta-\alpha$ of Figure 5a), and these values were almost consistent with that of **2** in the crystalline state. This finding was also indicative of the electronic interaction between the diimide **3** and the calculation of the Mulliken charge of **3** that was also conducted by the DFT method (B3LYP/6-311G**//B3LYP/6-31G*). As expected, the carbon atoms at the 3- and 6-positions, the adjacent sp^2 carbon atoms of phenylacetylene, and the carbonyl oxygen atoms of **3** were negatively charged with the values of −0.29, −0.20, and −0.31, respectively. On the other hand, the carbonyl carbon atoms and the adjacent sp carbon atoms of the diimide moiety were found to be positively charged with the values of +0.45 and +0.14, respectively. Thus, the packing arrangement of **3** is also interpreted by the possible electrostatic interaction caused by the introduction of the phenylacetylene moiety, in which the difference in the electrostatic interactions in **3** would provide the two kinds of stacking patterns of $\alpha-\beta$ and $\beta-\alpha$ in Figure 5a. In addition to the analogous contacts in the case of **2**, the further electrostatic interaction between the carbon atom at the 3-position in the diimide and the adjacent sp carbon atom was observed in the stacking pattern of $\alpha-\beta$ in **3**.

The packing diagram of $(\mathbf{3})_2$·*p*-xylene in Figure 5b shows that **3** exhibited a slanted stacking aligned *a*-axis and the multipoint C−H···O interactions between the carbonyl oxygen and the phenyl hydrogen atoms with the C−H···O distance of 2.47 (A of Figure 5b) and 2.60 (B of Figure 5b) Å. The *p*-xylene molecules served as adhesive to interact with **3** by C−H···π interactions[33] with the distance of 2.94 (C of Figure 5b) and 2.88 (D of Figure 5b) Å.

Photophysical Properties. The UV/vis and fluorescence spectra of **1**−**3** were measured in $CHCl_3$ and toluene to investigate the influence of the solvent polarity on the optical properties. These data are summarized in Table 1. The UV/vis spectra in $CHCl_3$ of **1**−**3** are shown in Figure 6. Compared to **1**, the longer wavelength absorption maxima of **2** and **3** were significantly shifted bathochromically by ca. 70 nm, and their absorption coefficients (ϵ) dramatically increased due to the linear 1D π-system on the pyromellitic diimide moiety. The macrocycle **2** [359 (ϵ 89400), 380 (ϵ 78000), 427 (ϵ 8700, sh)] and acyclic **3** [356 (ϵ 47600), 376 (ϵ 66800), 414 (ϵ 5800, sh)] in $CHCl_3$ solution exhibited similar spectra with two absorption maxima (λ_{max}) and one shoulder above 400 nm. The transannular

(31) The crystal packing of dehydro[12]annulene fused with tetrafluorobenzne, in which one of the tetrafluorobenzene rings faced the annulene core of another molecule, was rationalized with its Mulliken charge by using B3LYP/6-31G(d) level of theory by Komatsu et al., see: Nishinaga, T.; Nodera, N.; Miyata, Y.; Komatsu, K. *J. Org. Chem.* **2002**, *67*, 6091–6096.

(32) It was reported that *N*,*N*′-di(2-*tert*-butylphenyl)-3,6-di(4-chlorophneyl)-pyromellitic diimide did not exhibit the intermolecular $\pi-\pi$ interactions in the crystalline state due to the bulky *tert*-butylphenyl groups.[16]

(33) Nishio, M.; Hirota, M.; Umezawa, Y. *The CH/π interactions*; Wiley-VCH: New York, 1998.

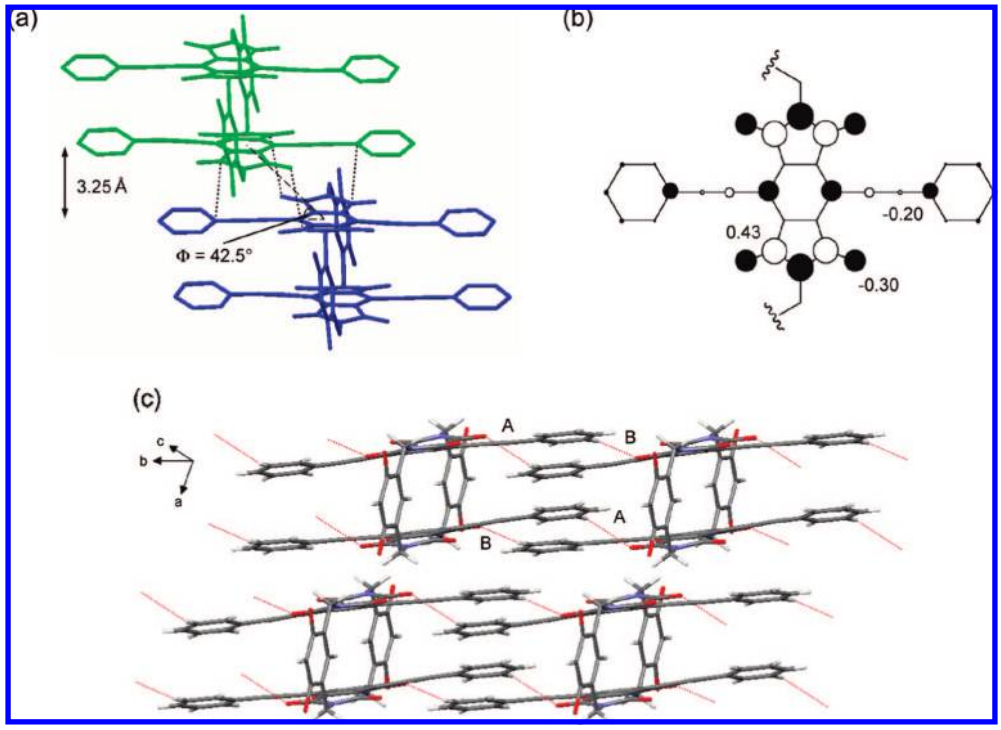

FIGURE 3. (a) Side view of packing arrangement of **2**. Dotted lines show within the sum of van der Waals radius and possible electrostatic interactions. (b) Sketches with the Mulliken charge of **2′** at the B3LYP/6-311G**//B3LYP/6-31G* level: light and dark colors indicate positively and negatively charged atoms, respectively; the diameters of the circles are in proportion to the values of charge distribution. (c) Packing diagram of **2**. Dotted lines show C−H···O interactions. Octyl groups of **2** are omitted for clarity. Selected distances (Å) of dotted lines: A, 2.67; B, 2.42.

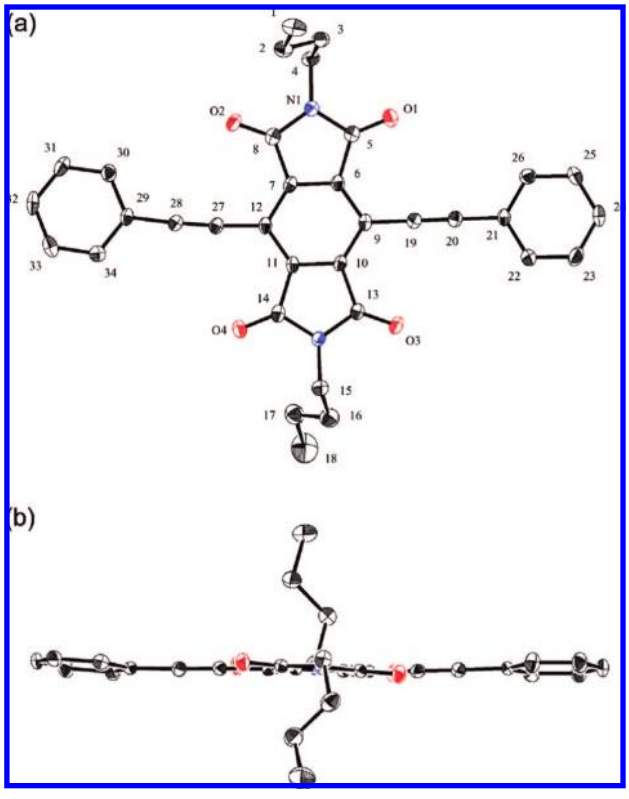

FIGURE 4. ORTEP drawing of the (a) top view and (b) side view of $(\mathbf{3})_2 \cdot p$-xylene. Thermal ellipsoids are drawn at the 50% probability level. Hydrogen atoms and the *p*-xylene molecule are omitted for clarity.

interaction of the pyromellitic diimide moieties in **2** might be negligible in the ground state because the absorption bands of **2** appeared at almost the same positions as those of **3**, whereas the intensities of the absorption bands of **2** were higher than those of the corresponding bands of **3**. The λ_{max} values of **2** and **3** were scarcely changed between the nonpolar toluene and more polar $CHCl_3$ (Table 1).

The electronic transitions of the pyromellitic diimide-based π-conjugated compounds structurally modified at the 3- and 6-positions have not been studied in detail, while those in the pyromellitic diimide chromophore were well-documented by Gawroński, Gawrońska, Koput, and Rychlewska's group.[34] Therefore, we calculated the frontier molecular orbitals (FMOs) of **2′** and **3** and their electronic transitions by the TDDFT method at the B3LYP/6-31G* level of theory for their optimized structures (B3LYP/6-31G*). As summarized in Table 1, this level of calculations almost reproduced the UV/vis spectra of **2** and **3**, predicting the absorption at 389 and 498 nm in **2** and 397 and 498 nm in **3**. It is considered that the observed split of the absorption bands around 340−400 nm in **2** and **3** was derived from the vibrational structures.

Figure 7 shows the relationship between the electronic transitions and the FMO plots of **2′** and **3**. For **3**, the calculations predicted that the absorption bands around the shorter and longer wavelength regions were essentially assigned to the transition from the HOMO delocalized over the bis(phenylethynyl)pyromellitic diimide moiety to the similarly delocalized LUMO+1 and the transition from the HOMO to the LUMO mainly localized on the pyromellitic diimide moiety, respectively. The larger oscillator strength of the HOMO → LUMO+1 transition compared to that of HOMO → LUMO agreed well with the trend in the observed ϵ values. The FMOs of **2′** closely

(34) Gawroński, J.; Brzostowska, M.; Gawrońska, K.; Koput, J.; Rychlewska, U.; Skowronek, P.; Nordén, B. *Chem. Eur. J.* **2002**, *8*, 2484–2494.

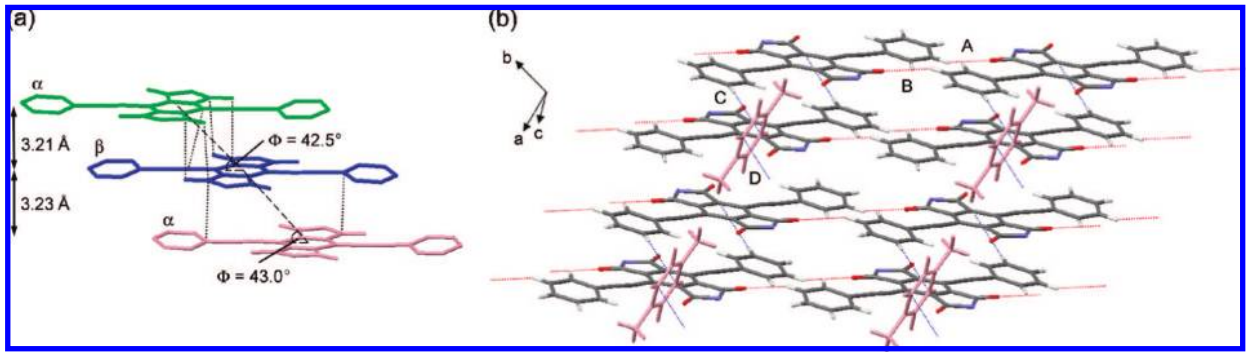

FIGURE 5. (a) Side view of the packing arrangement of $(\mathbf{3})_2 \cdot p$-xylene. Dotted lines show within the sum of van der Waals radius and possible electrostatic interactions. (b) Packing diagram of $(\mathbf{3})_2 \cdot p$-xylene. Dotted red and blue lines show C−H···O and C−H···π interactions, respectively. Butyl groups of **3** are omitted for clarity. Selected distances (Å) of dotted lines: A, 2.47; B, 2.60; C, 2.94; D, 2.88.

TABLE 1. Electronic Absorption and Emission Data for 1−3

compd	solvent	λ_{max} [nm] (ϵ [M^{-1} cm^{-1}])	calcd λ_{max} [nm] (f)[a]	λ_{em} [nm[b]] (Φ_f)
1	$CHCl_3$	285 (10600), 305 (5400)[c]		488 (0.001)[d]
2	$CHCl_3$	359 (89400), 380 (78000), 427 (sh, 8700)	389 (2.513), 498 (0.095)[e]	461, 592 (0.002)[f]
	toluene	357 (98200), 378 (83600), 427 (sh, 9300)		442, 467, 583 (0.004)[f]
3	$CHCl_3$	356 (47600), 376 (66800), 414 (sh, 5800)	397 (1.446), 498 (0.051)	492 (0.11)[f]
	toluene	353 (47300), 375 (67500), 414 (sh, 7500)		477 (0.11)[f]

[a] TDDFT (TD/B3LYP/6-31G*) calculations were carried out with use of optimized structures at the B3LYP/6-31G* level of theory. [b] Measured in 1 × 10^{-6} M solution. [c] Reference 17b. [d] Fluorescence quantum yield relative to anthracene. [e] In **2′**, which replaced the octyloxy groups in **2** with methoxy groups. [f] Fluorescence quantum yield relative to quinine bisulfate.

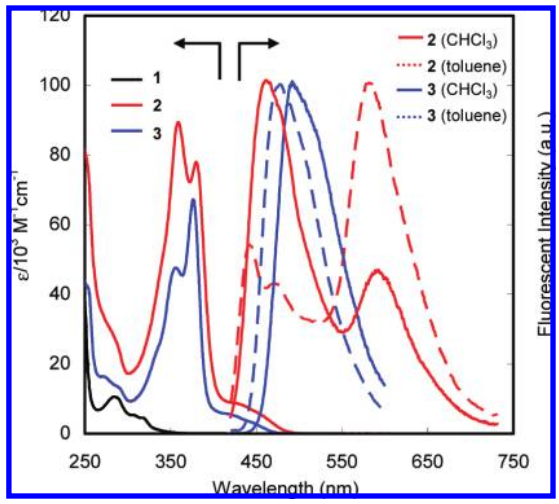

FIGURE 6. Electronic absorption of **1**−**3** in $CHCl_3$ solution and emission spectra of **2** and **3**.

resembled those of **3** but the three FMOs of **3**, HOMO, LUMO, and LUMO+1, split into the six FMOs of **2′** presumably due to the inversion of the orbitals of the bis(phenylethynyl)pyromellitic diimide moiety across the xylyl moiety; the HOMO, LUMO, and LUMO+1 of **3** corresponded to HOMO−3 and HOMO−2, LUMO and LUMO+1, and LUMO+2 and LU-

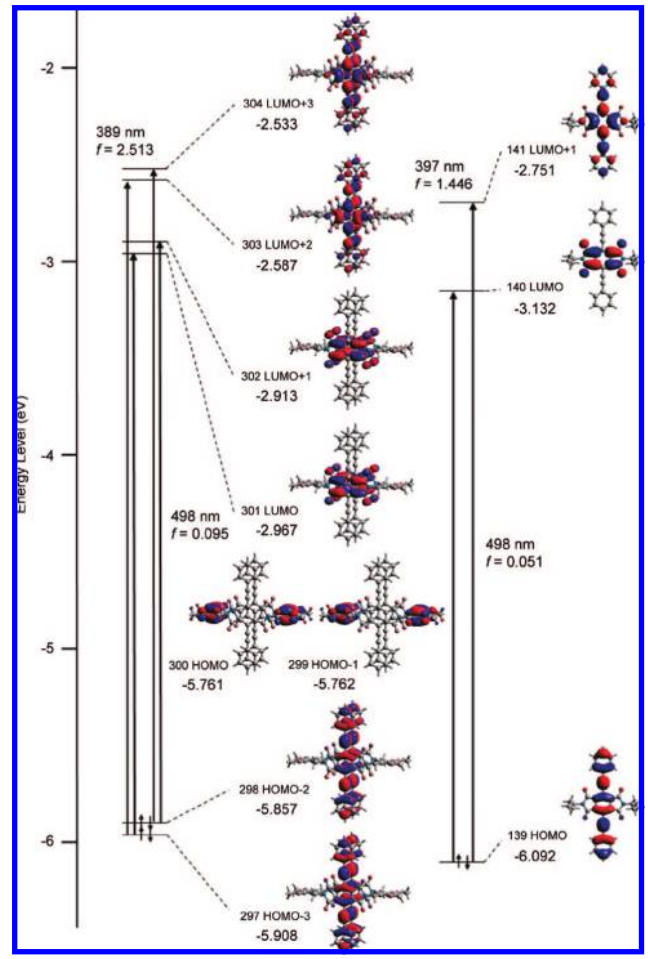

FIGURE 7. Selected frontier molecular orbitals for **2′** (left) and **3** (right) calculated at the B3LYP/6-311G**//B3LYP/6-31G* level of theory. Absorption wavelength and oscillator strength were calculated by TDDFT (TD/B3LYP/6-31G*).

MO+3, respectively, of **2′**. Analogous to the electronic transitions of **3**, the absorption bands around the shorter and longer wavelength regions of **2** were ascribed to the transitions of HOMO−3 → LUMO+2 and HOMO−2 → LUMO+3 and the transitions of HOMO-3 → LUMO and HOMO−2 → LUMO+1, respectively. Meanwhile, the HOMO and HOMO+1 of **2′** were localized on the electron-rich xylyl moieties.

Figure 6 also shows the fluorescence spectra of **2** and **3** in toluene and $CHCl_3$. The acyclic **3** emitted a green fluorescence at the wavelength region of ca. 470−540 nm with a moderate

fluorescence quantum yield (Φ_f 0.11 in both toluene and $CHCl_3$). With the increasing solvent polarity, the emission maxima (λ_{em}) of **3** showed a bathochromic shift from 477 nm in toluene to 492 nm in $CHCl_3$, suggesting that the excited state was slightly stabilized by solvation in the relatively polar $CHCl_3$. Contrary to the absorption process, the fluorescence properties were significantly different between **2** and **3**. The macrocycle **2** showed a fluorescence in the significantly longer wavelength region of 583 nm in toluene and 592 nm in $CHCl_3$ in addition to the shorter wavelength fluorescence that might essentially correspond to that of **3**. Furthermore, the Φ_f values of **2** in both toluene (0.004) and $CHCl_3$ (0.002) were dramatically lower than those of **3**. To investigate the effect of the macrocyclic structure or phenylacetylene groups of **2** on its fluorescence properties, we also measured the fluorescence spectra of the macrocycle **1** and *N*,*N*′-di-*n*-butylpyromellitic diimide.[35,36] The fluorescence spectrum of **1** was similar to that of the *N*,*N*′-di-*n*-butylpyromellitic diimide and the additional longer wavelength fluorescence was not observed in **1** up to 700 nm despite its macrocyclic structure (Figure S17 and Table S1, Supporting Information). The Φ_f values of both **1** and *N*,*N*′-di-*n*-butylpyromellitic diimide were very small (0.001−0.005). Considering these findings, one can conclude that the observed fluorescence in the longer wavelength region of **2** was ascribed to the excimer emission of the bis(phenylethynyl)pyromellitic diimide moieties because the intramolecular aromatic interactions are expected to be due to the rotation of the sp carbons of the phenylacetylene groups. These spectroscopic data are in good agreement with the structural features found in the X-ray crystallography of **2** as already described. The fluorescence emission of **2** in toluene was observed as a mirror image of the absorption at 442 and 467 nm, which might be caused by the rigid macrocyclic structure of **2**.

Redox Properties. To examine the effect of the 1D π-system on the redox behavior of the pyromellitic diimide derivatives, cyclic voltammetries of **1**−**3** and *N*,*N*′-di-*n*-butylpyromellitic diimide were conducted in CH_2Cl_2 with tetra-*n*-butylammonium hexafluorophosphate as the supporting electrolyte at room temperature. The voltammograms are shown in Figure 8 and the values of the reduction potentials and LUMO energies are summarized in Table 2. It has been well-documented that pyromellitic diimide derivatives form the radical anion and dianion as stable species by two reversible one-electron reductions.[36] For example, *N*,*N*′-di-*n*-butylpyromellitic diimide exhibited two reversible one-electron reductions at −1.35 and −1.92 V vs Fc/Fc^+, and the first and second waves were ascribed to the radical anion and dianion species, respectively (Figure 8). Reversible redox processes were also observed in **1**−**3**. In **3**, two analogous reversible one-electron reductions were observed at −1.28 and −1.84 V, which were more positive potentials relative to those of the *N*,*N*′-di-*n*-butylpyromellitic diimide by ca. 70−80 mV, but the DFT calculations (B3LYP/6-311G**//B3LYP/6-31G*) indicated that the calculated LUMO level of **3** was slightly higher than that of *N*,*N*′-di-*n*-butylpyromellitic diimide by ca. 0.19 eV as summarized in Table 2. Thus, these observations might be attributed to the solvation that causes the shift of the reduction potentials.

In our previous study, we found that the first two-electron reduction wave of **1** was split into two waves due to the electrostatic repulsion between the radical anion and the neutral pyromellitic diimide moiety. The macrocycle **2** also exhibited a reduction wave similar to that of **1**. However, the split range of the first reduction wave of **2** increased compared to that of **1** by ca. 60 mV and the second reduction wave of **2** shifted toward a more negative potential by ca. 70 mV than that of **1**. These observations indicated that the increase in the number of π-electrons in **2** provided a stronger electrostatic repulsion between the radical anion and the neutral diimide in the first reduction process and between the further reduced species in the second reduction process; the electrostatic repulsions of the radical anion−radical anion and dianion−radical anion were expected.

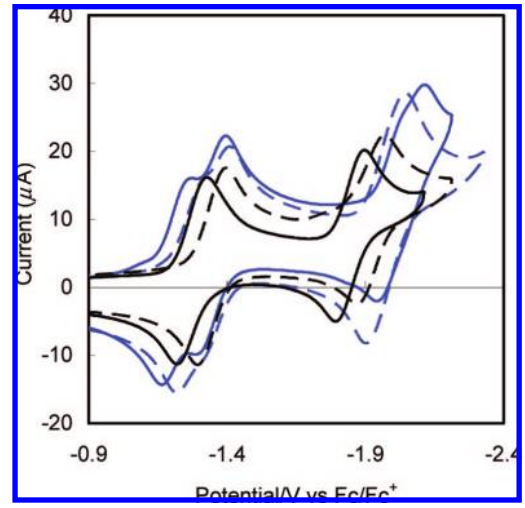

FIGURE 8. CV traces for **1** (dashed blue line), **2** (solid blue line), *N*,*N*′-di*n*-butylpyromellitic diimide (dashed black line), and **3** (solid black line).

TABLE 2. Potentials (V vs Fc/Fc^+) for the Reduction Processes[a] and LUMO Levels at the B3LYP/6-311G//B3LYP/6-31G* Level of 1−3 and *N*,*N*′-Di-*n*-butylpyromellitic Diimide**

compd	$^1E_{1/2}$		$^2E_{1/2}$	LUMO (eV)
1	−1.28	−1.35	−1.96	−3.240
2	−1.21	−1.34	−2.03	−2.967[b]
N,*N*′-di-*n*-butylpyromellitic diimide	−1.35		−1.92	−3.324
3	−1.28		−1.84	−3.132

[a] All electrochemical measurements were performed in CH_2Cl_2 solution containing 0.10 M tetra-*n*-butylammonium hexafluorophosphate at a scan rate of 200 mV s^{-1}. [b] In **2′**, which replaced the octyloxy groups in **2** with methoxy groups.

Complexation Studies. It is well-known that the pyromellitic diimide derivatives form the CT complexes with π-donors in solution. Consequently, we carried out the UV/vis spectral titration experiments with **3** in the presence of various π-donors in concentrated $CHCl_3$ solution (**3**: 1.0×10^{-3} M) to investigate the effect of the linear 1D π-system on the CT complex formation. As π-donor guests, aniline, *p*-dimethoxybenzene, α-naphthol, and indole were chosen. Additional CT bands should appear in the intermolecular CT complex between **3** as an acceptor and a donor guest. In every case, the addition of an excess amount of the π-donors to **3** produced an enhancement in the end absorption around 480−550 nm, which was assigned to the CT band from the π-donors to **3**. For example, the UV/vis spectral change in Figure 9a showed a monotonic growth of the diagnostic CT absorbance upon the incremental addition of the indole to **3** at 25 °C. These findings indicated the CT complex formation between **3** and aniline, *p*-dimethoxybenzene,

(35) Buchwalter, S. L.; Iyengar, R.; Viehbeck, A.; O'Toole, T. R. *J. Am. Chem. Soc.* **1991**, *113*, 376–377.
(36) Carroll, J. B.; Gray, M.; McMenimen, K. A.; Hamilton, D. G.; Rotello, V. M. *Org. Lett.* **2003**, *5*, 3177–3180.

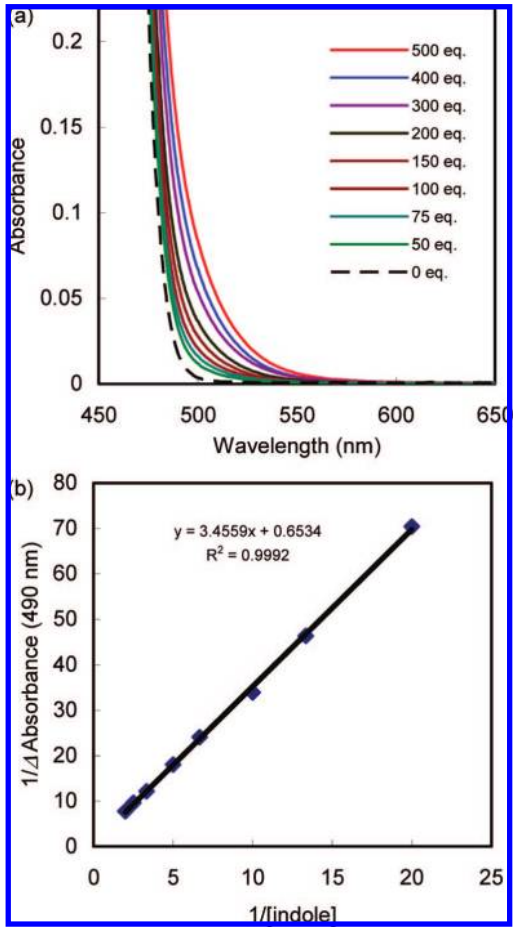

FIGURE 9. (a) Absorption spectra of **3** in $CHCl_3$ at 1×10^{13} M in the presence of 0−500 equiv of indole. (b) Benesi−Hildebrand plot.

TABLE 3. Charge-Transfer Association and HOMO/LUMO Energy Levels of 3 and π-Donors[a]

compd	K_{CT}[b]	HOMO (eV)	LUMO (eV)
3		−6.092	−3.132
aniline	0.1 (0.1[c])	−5.639	+0.121
p-dimethoxybenzene	0.2 (0.3[d])	−5.508	−0.300
α-naphthol	0.4 (1.0[d])	−5.683	−1.084
indole	0.2 (1.0[d])	−5.666	−0.410

[a] HOMO and LUMO energy levels were calculated by using the B3LYP/6-311G**//B3LYP/6-31G* level of theory. [b] In $CHCl_3$ containing 1 mM **3** and 50−6000 mM π-donors at 25 °C, whereas the value in parentheses is for **1**. [c] Reference 17c. [d] Reference 17b.

α-naphthol, and indole (Figures S18−S20, Supporting Information). The HOMO and LUMO energies of **3** and the π-donors are summarized in Table 3. The observed CT complex formation was rationalized by the calculated HOMO and LUMO energy levels. Thus, the calculated HOMO energy of **3** was lower than those of aniline, *p*-dimethoxybenzene, α-naphthol, and indole, while the LUMO energy of **3** was remarkably lower than those of the π-donors. For qualitative analysis of the CT interaction in solution, the spectrophotometric changes were treated by the Benesi-Hildebrand procedures[37] as shown in Figure 9b, which extracted the association constants (K_{CT}) of **3** with the π-donors: K_{CT} = 0.1 for aniline, 0.2 for *p*-dimethoxybenzene, 0.4 for α-naphthol, and 0.2 for indole (Table 3), which were comparable to those of **1** with various π-donors as previously reported by our group.[17b] It is considered that the low K_{CT} values are related to the finding that the LUMO of **3**, which interacts with the HOMOs of the π-donors during the CT complex formation process, localizes at the pyromellitic diimide moiety (Figure 7) and the phenylacetylene groups scarcely affect the stabilization of their CT complexes.

Clathrate Compounds of 3 and π-Donors. Since the UV/vis spectral experiments strongly suggested the CT complex formation with **3** and various π-donors, we examined the solid state structures. Slow recrystallization of **3** from the aniline solution gave single crystals of **3**·aniline suitable for an X-ray crystallographic analysis. The slow evaporation of the CH_2Cl_2 solution of **3** in the presence of *p*-dimethoxybenzene gave **3**·(*p*-dimethoxybenzene)$_2$. Similarly, the recrystallization of **3** from $CHCl_3$ in the presence of α-naphthol and indole by vapor diffusion with hexane gave **3**·α-naphthol and **3**·(indole)$_2$, respectively. We presumed that a coprecipitation effect contributed to the formation of the clathrate compounds because the 1:1 CT complexes were expected in $CHCl_3$ solution based on the UV/vis spectral titration study. In the crystal of **3**·α-naphthol, α-naphthols exhibited a 50% static disorder.

Figure 10 shows the packing diagram of the clathrate compounds of **3** with the π-donors of aniline, *p*-dimethoxybenzene, α-naphthol, and indole (Figure S21−S24 for their ORTEP drawings, Supporting Information). On the basis of the investigation of the UV/vis spectral titration study, a D (donor)−A (acceptor) orbital overlap was expected as in the case of the clathrates of **1**[17b] or *N*,*N*′-bis(2-*tert*-butylphenyl)pyromellitic diimide.[38] However, the X-ray crystallographic analyses disclosed unexpected packing patterns, in which **3** as an acceptor stacked in a parallel and slanted arrangement formed the segregated D−A structures in all cases. The angles between the plane of the diimide **3** and the stacking axis were 43.1° and 43.2° in **3**·aniline, 42.5 and 42.6° in (**3**)$_2$·*p*-dimethoxybenzene, 41.9° in **3**·α-naphthol, and 45.3° in **3**·(indole)$_2$. The intermolecular distances (*d*) between the center of the diimide and the π-face of the facing diimide were shorter than the sum of the van der Waals radii of the two sp^2 carbons: *d* = 3.20 and 3.21 Å in **3**·aniline, 3.21 and 3.27 Å in (**3**)$_2$·*p*-dimethoxybenzene, 3.16 Å in **3**·α-naphthol, and 3.21 Å in **3**·(indole)$_2$. In all cases, the donor molecules were located in close proximity to **3** (Figures S25−S28, Supporting Information). For the aniline and α-naphthol clathrates, which are hydrogen bonding donors, the hydrogen bonding was observed with the N−H···O distance of 2.54 Å and the O−H···O distance of 1.93 Å in **3**·aniline (Figure S25, Supporting Information) and **3**·α-naphthol (Figure S27), respectively. In addition to the hydrogen bonding, there were C−H···O interactions with the C−H (aromatic)···O (carbonyl) distances of 2.65 and 2.79 Å in **3**·aniline (Figure S25, Supporting Information) and with the C−H (aromatic)···O (hydroxy) distance of 2.54 Å in **3**·α-naphthol (Figure S27, Supporting Information). Similarly, the C−H···O interactions were observable with the C−H (aromatic)···O (carbonyl) and the C−H (methyl)···O (carbonyl) distances being 2.46 and 2.56 Å, respectively, in (**3**)$_2$·*p*-dimethoxybenzene (Figure S26, Supporting Information), and were also observable with the C−H (aromatic)···O (carbonyl) distances being 2.37 Å in **3**·(indole)$_2$ (Figure S28, Supporting Information). However, the interactions between the π-donors in these crystals depended on the size of their

(37) (a) Benesi, H. A.; Hildebrand, J. J. *J. Am. Chem. Soc.* **1949**, *71*, 2703–2707. (b) Person, W. B. *J. Am. Chem. Soc.* **1965**, *87*, 167–170.

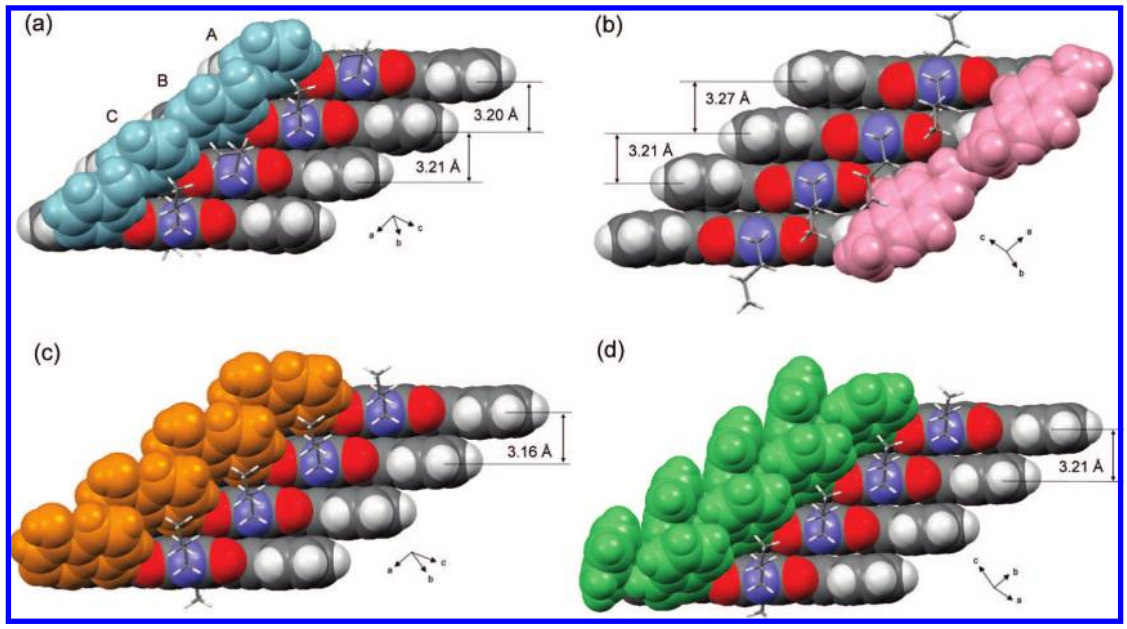

FIGURE 10. Packing diagrams of clathrate compounds of **3** with π-donors: (a) **3**·aniline (light blue), (b) (**3**)$_2$·*p*-dimethoxybenzene (pink), (c) **3**·α-naphthol (orange), and (d) **3**·(indole)$_2$ (light green).

π surfaces. In the crystal of **3**·aniline, the aniline molecules adopted an aniline dimer geometry (anilines A and B in Figure 10a) by self-complementary N−H···π interactions with the shortest N−H···C (aromatic) distance of 2.99 Å (Figure S25, Supporting Information). The distance between the centers of the aniline π-planes (aniline B and C in Figure 10a) was 5.87 Å and the closest C−C distance was 3.69 Å, indicating that the electronic interaction between these aniline dimer structures might be negligibly small if any. In the crystal of (**3**)$_2$·*p*-dimethoxybenzene, the electronic interaction between two *p*-dimethoxybenzenes should be entirely negligible (Figure 10b and Supporting Information Figure S26). In contrast, there were definite interactions between the π-donors in the crystals of **3**·α-naphthol and **3**·(indole)$_2$. In **3**·α-naphthol, the angle of the centers of the α-naphthol π-planes and the stacking axis was 38.9° and the distance of the π-planes was about 3.4 Å, indicating an electronic interaction between the α-naphthols (Figure 10c and Supporting Information Figure S27). In **3**·(indole)$_2$, the indole molecules were shown to have a zigzag geometry by a combination of the N−H···π interactions with the short N−H···C distances of 2.45 and 2.48 Å and C−H···π interactions with the short C−H···C distances of 2.45, 2.48, and 2.84 Å (Figure 10d and Supporting Information Figure S28).

Considering the finding that **3** in these clathrates stacked in a parallel and slanted arrangement with the interfacial distance below the sum of the van der Waals radii of two sp^2 carbons even in the presence of π-donors, this was indicative of the strong aggregation ability of **3** in the solid state. Thus, the stabilization by this type of attractive $\pi-\pi$ interaction of **3** in the solid state, which clearly resembled that in the (**3**)$_2$·*p*-xylene, would exceed the stabilization by the expected D−A orbital interactions regardless of the size of their π-surfaces. The crystal packing of **3** in these clathrates also could be interpreted by the possible electrostatic interactions expected from the Mulliken charge of **3** by DFT calculations as is the case of the (**3**)$_2$·*p*-xylene (Figure 11b). For example, in **3**·aniline, the closest intermolecular contacts were observed between the carbonyl

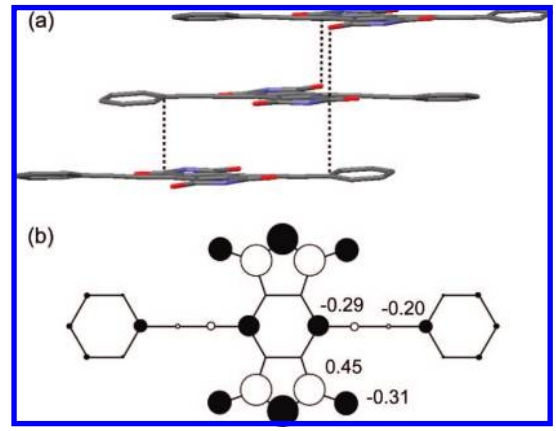

FIGURE 11. (a) Side view of the arrangement of **3**·aniline. Dotted lines show within the sum of van der Waals radius and possible electrostatic interactions. Butyl groups of **3**, aniline molecules, and hydrogen atoms are omitted for clarity. (b) Sketches with the Mulliken charge of **3** calculated at the B3LYP/6-311G**//B3LYP/6-31G* level: light and dark colors indicate positively and negatively charged atoms, respectively; the diameters of the circles are in proportion to the values of the charge distribution.

carbons (+0.45) and the carbonyl oxygens (−0.31), and between the carbonyl carbons and the sp^2 benzene carbons (−0.20) (Figure 11a). Similar intermolecular contacts were observable in all cases, although their stacking arrangements slightly differed depending on the π-donors (Figure S29, Supporting Information). The strong aggregation tendency of the bis(phenylethynyl)pyromellitic diimide moiety was also supported by the MALDI-TOF mass spectrum of **3**, in which the apparent intensity peak was observed at three multiples (1584) of the parent ions at *m*/*z* 528 (Figure S30, Supporting Information). In contrast to the observed aggregation in the solid state, the monomeric form of **3** was present in the solution even at 10 mM as revealed by the ^{1}H NMR spectra of **3** in $CDCl_3$ at room temperature (Figure S31, Supporting Information). The signal of the aromatic protons at 7.33−7.38 and 7.75 ppm showed no

significant shifts indicating the existence of only a weak $\pi-\pi$ interaction in solution.

3. Conclusions

In conclusion, we have synthesized a novel pyromellitic diimide-based macrocycle with a linear π-electronic system **2** and *N*,*N*′-di-*n*-butyl-3,6-bis(phenylethynyl)pyromellitic diimide **3**. The X-ray crystal structures and theoretical calculations of **2**, **2′**, and/or **3** and the clathrate formations of **3** with π-donors indicated the presence of significant electrostatic interactions between the bis(phenylethynyl)pyromellitic diimide moiety in the solid state, which was supported by the MALDI-TOF mass spectral measurement of **3**. The transannular $\pi-\pi$ interactions of the bis(phenylethynyl)pyromellitic diimide moieties in **2** were expected to be very weak in the ground state, but **2** and **3** showed quite different excited state properties. The macrocycle **2** showed an excimer fluorescence in toluene and $CHCl_3$. Furthermore, the cyclic voltammetry measurements for **1**−**3** and *N*,*N*′-di-*n*-butylpyromellitic diimide revealed that an increase in the number of π-electrons in this type of macrocyclic structure provided the enhancement of their electrostatic repulsion between the diimide moieties. On the basis of the observed results, we expect the bis(phenylethynyl)pyromellitic diimide moiety with elongated π-system, aggregation ability, and electronic affinity as a new n-type structural motif for the preparation of organic field-effect transistor (OFET) materials. We also plan to prepare a new covalent organic nanotube[39] with an extended 1D π-system by the introduction of ethynyl-substituted pyromellitic diimide derivatives to the tetrabromide **10**. Our synthetic study is now in progress and the results will be reported elsewhere. We believe that the present study provides valuable information for the creation of pyromellitic diimide-based π-electron materials.

4. Experimental Section

Phenylethynyl-Substituted [2 + 2] Pyromellitic Diimide-Based Macrocycle (2). A flask was charged with the macrocycle **10** (150 mg, 0.10 mmol), $PdCl_2(PPh_3)_2$ (14 mg, 2.06 μmol), and CuI (7 mg, 3.29 μmol) in THF/Et_3N (1:1, 12 mL). The mixture was degassed by bubbling nitrogen for 30 min and a solution of phenylacetylene (63 mg, 0.62 mmol) in THF (1 mL) was added. After the mixture was heated at 75 °C for 36 h under a nitrogen atmosphere, the reaction mixture was concentrated in vacuo to dryness. The residue was purified by silica gel column chromatography eluting with $CHCl_3$/hexane (2:1, v/v) and preparative TLC with $CHCl_3$/hexane (1:4, 1:3, 1:2, 2:3, v/v) to give **2** in 23% yield (35 mg, 0.023 mmol) as a yellow powder. An analytical sample was obtained by recrystallization from $CHCl_3$/hexane: mp >300 °C; IR (KBr) ν_{max} 3471, 2925, 2855, 2210 ($\nu_{C\equiv C}$), 1766 ($\nu_{C=O}$), 1725 ($\nu_{C=O}$), 1623, 1510, 1385, 1303, 1184, 1115 cm^{-1}; ^1H NMR (300 MHz, $CDCl_3$) δ 0.81 (t, J = 7.0 Hz, 12 H), 1.23−1.38 (m, 32 H), 1.38−1.50 (m, 16 H), 1.78 (tt, J = 6.4 Hz, 8 H), 3.97 (t, J = 6.4 Hz, 8 H), 4.82 (s, 8 H), 6.14 (s, 2 H), 6.43 (s, 2 H), 6.98−7.11 (m, 12 H), 7.44 (d, J = 6.6 Hz, 8 H); ^{13}C NMR (75 MHz, $CDCl_3$) δ 14.1, 22.7, 26.1, 29.25, 29.30, 29.38, 29.7, 31.8, 36.6, 68.4, 80.9, 106.3, 114.6, 115.0, 120.7, 121.7, 128.0, 129.6, 132.7, 135.5, 156.0; MALDI-TOF-MS (dithranol) *m*/*z* calcd for $C_{100}H_{100}N_4O_{12}$ 1548.73 (M^+), found 1548.62. Anal. Calcd for $C_{100}H_{100}N_4O_{12}\cdot 0.15CHCl_3$: C, 76.72; H, 6.43; N, 3.57. Found: C, 76.75; H, 6.42; N, 3.65.

***N*,*N*′-Di-*n*-butyl-3,6-bis(phenylethynyl)pyromellitic Diimide (3).** A flask was charged with the dibromide **11** (473 mg, 0.97 mmol), $PdCl_2(PPh_3)_2$ (41 mg, 0.058 mmol), and CuI (22 mg, 0.12 mmol) in THF/Et_3N (1:1, 30 mL). The mixture was degassed by bubbling nitrogen for 30 min and a solution of phenylacetylene (227 mg, 2.23 mmol) in THF (3 mL) was added. After the mixture was heated at 75 °C for 12 h under a nitrogen atmosphere, the reaction mixture was concentrated in vacuo to dryness, suspended in CH_2Cl_2 (100 mL), and filtered through a bed of silica gel. The filtrate was concentrated and purified by silica gel column chromatography eluting with $CHCl_3$/hexane (4:1, v/v) and preparative TLC eluting with $CHCl_3$/hexane (1:4, 1:3, 2:3, v/v) to give **3** in 72% yield (315 mg, 0.60 mmol) as a yellow powder. An analytical sample was obtained by recrystallization from CH_2Cl_2/hexane: mp >300 °C; IR (KBr) ν_{max} 3457, 2932, 2212 ($\nu_{C\equiv C}$), 1765 ($\nu_{C=O}$), 1707 ($\nu_{C=O}$), 1507, 1402, 1369, 1340, 1170, 1058 cm^{-1}; ^1H NMR (300 MHz, $CDCl_3$) δ 0.90 (t, J = 7.3 Hz, 6 H), 1.35 (qt, J = 7.3 Hz, 4 H), 1.66 (tt, J = 7.3 Hz, 4 H), 3.69 (t, J = 7.3 Hz, 4 H), 7.33−7.38 (m, 6 H), 7.75 (pseudo dd, J = 2.0, 7.2 Hz, 4 H); ^{13}C NMR (75 MHz, $CDCl_3$) δ 13.6, 20.2, 30.5, 38.4, 81.5, 105.1, 115.0, 122.9, 128.5, 130.0, 132.7, 136.2, 164.8; FAB-MS (NBA, positive) 529 [$(M + H)^+$]. Anal. Calcd for $C_{34}H_{28}N_2O_4$: C, 77.25; H, 5.35; N, 5.30. Found: C, 77.08; H, 5.35; N, 5.30.

1,3-Di-*n*-octyloxy-4,6-diiodobenzene (6). To a solution of 1,3-dioctoxybenzene **5** (50.0 g, 146 mmol) in AcOH (800 mL) was added dropwise iodine monochloride (50.0 g, 308 mmol) and the solution was stirred at room temperature for 3 h. The reaction mixture was poured into water (800 mL) and extracted with $CHCl_3$. The combined organic layers were washed with aqueous $Na_2S_2O_3$ and saturated aqueous $NaHCO_3$, dried over anhydrous $MgSO_4$, and evaporated in vacuo to dryness. The residue was purified by silica gel column chromatography eluting with hexane, followed by recrystallization from hexane to give **6** in 92% yield (78.7 g, 134 mmol) as colorless needles: mp 63−64 °C; IR (KBr) ν_{max} 2954, 2927, 2854, 1567, 1556, 1483, 1456, 1403, 1388, 1355, 1272, 1199, 1064, 1033 cm^{-1}; ^1H NMR (300 MHz, $CDCl_3$) δ 0.99 (t, J = 7.3 Hz, 6 H), 1.49−1.62 (m, 4 H), 1.77−1.86 (m, 4 H), 3.99 (t, J = 6.4 Hz, 4 H), 6.32 (s, 1 H), 8.02 (s, 1 H); ^{13}C NMR (75 MHz, $CDCl_3$) δ 14.3, 22.8, 26.2, 29.2, 29.3, 29.4, 69.7, 76.2, 98.0, 146.8, 159.2; FAB-MS (NBA, positive) 586 (M^+). Anal. Calcd for $C_{22}H_{36}I_2O_2$: C, 45.18; H, 6.15. Found: C, 45.07; H, 6.19.

1,3-Di-*n*-octyloxy-4,6-dicyanobenzene (7). A solution of the iodide **6** (12.0 g, 20.5 mmol) and CuCN (5.50 g, 61.4 mmol) in NMP (40 mL) was heated at 150 °C for 10 h under a nitrogen atmosphere. The reaction mixture was poured into a 1.2 N HCl solution (150 mL) of iron chloride (33.5 g, 205 mmol) and stirred at 60 °C for 4 h. The precipitates were collected by filtration and washed well with water. To this precipitate was added $CHCl_3$ (200 mL) and the solution was stirred for 1 h. The insoluble material was removed by filtration through Celite, and the filtrate was washed with aqueous $Na_2S_2O_3$, saturated $NaHCO_3$, and brine, dried over anhydrous $MgSO_4$, and evaporated in vacuo to dryness. The residue was purified by silica gel column chromatography eluting with $CHCl_3$/hexane (3:2, v/v) to give **7** in 59% yield (4.65 g, 12.1 mmol) as a white powder: mp 28−29 °C; IR (KBr) ν_{max} 2923, 2854, 2227 ($\nu_{C\equiv N}$), 1616, 1560, 1506, 1434, 1400, 1319, 1220, 1114, 993 cm^{-1}; ^1H NMR (300 MHz, $CDCl_3$) δ 0.89 (t, J = 7.0 Hz, 6 H), 1.28−1.52 (m, 20 H), 1.88 (tt, J = 6.4 Hz, 4 H), 4.12 (t, J = 6.4 Hz, 4 H), 6.43 (s, 1 H), 7.71 (s, 1 H); ^{13}C NMR (75 MHz, $CDCl_3$) δ 14.0, 22.6, 25.7, 28.6, 29.0, 29.1, 31.7, 69.9, 95.0, 96.4, 114.7, 138.8, 165.4; HR-FAB-MS (NBA, positive) *m*/*z* calcd for $C_{24}H_{37}N_2O_2$

(38) Kishikawa, K.; Tsubokura, S.; Kohmoto, S.; Yamamoto, M.; Yamaguchi, K. *J. Org. Chem.* **1999**, *64*, 7568–7578.

(39) For covalent organic nanotubes, see: (a) Harada, A.; Li, J.; Kamachi, M. *Nature* **1993**, *364*, 516–518. (b) Ikeda, A.; Shinkai, S. *Chem. Commun.* **1994**, 2375–2376. (c) Kammermeiter, S.; Herges, R. *Angew. Chem., Int. Ed.* **1996**, *35*, 2669–2671. (d) Kim, S. K.; Sim, W.; Vicens, J.; Kim, J. S. *Tetrahedron Lett.* **2003**, *44*, 805–809. (e) Kim, Y.; Mayer, M. F.; Zimmerman, S. C. *Angew. Chem., Int. Ed.* **2003**, *42*, 1121–1126. (f) Organo, V. G.; Leontiev, A. V.; Sgarlata, V.; Dias, H. V. R.; Rudkevich, D. M. *Angew. Chem., Int. Ed.* **2005**, *44*, 3043–3047. (g) Jin, W.; Fukushima, T.; Kosaka, A.; Niki, M.; Ishii, N.; Aida, T. *J. Am. Chem. Soc.* **2005**, *127*, 8284–8285. (h) Organo, V. G.; Sgarlata, V.; Firouzbakht, F.; Rudkevich, D. M. *Chem. Eur. J.* **2007**, *13*, 4014–4023.

385.2855 [(M + H)$^+$], found 385.2858. Anal. Calcd for $C_{24}H_{36}N_2O_2$: C, 74.96; H, 9.44; N, 7.28. Found: C, 75.10; H, 9.53; N, 7.31.

1,3-Bis(aminomethyl)-4,6-dioctyloxybenzene (8). To a solution of the nitrile **7** (2.00 g, 5.21 mmol) in dry toluene (10 mL) was added 1.0 M diisobutylaluminum hydride solution (52 mL, 52.0 mmol) at room temperature under a nitrogen atmosphere. After the mixture was heated at 110 °C for 4 h, the reaction mixture was diluted with toluene and treated with KF (12.1 g, 208 mmol) and water (2.80 g, 156 mmol) at 0 °C. After being vigorously stirred at room temperature for 30 min, the suspension was filtered and washed with toluene. The filtrate was dried over anhydrous $MgSO_4$ and evaporated in vacuo to dryness to give **8** in 53% yield (1.08 g, 2.76 mmol) as a colorless oil. Without further purification, it was used in the next reaction: IR (NaCl) ν_{max} 3376 (ν_{NH_2}), 3290 (ν_{NH_2}), 1614, 1589, 1506, 1467, 1417, 1378, 1290, 1193, 1110, 1058 cm^{-1}; ^{1}H NMR (300 MHz, DMSO-d_6) δ 0.85 (t, J = 6.8 Hz, 6 H), 1.20−1.64 (m, 20 H), 1.67 (tt, J = 6.4 Hz, 4 H), 3.33 (s, 4 H), 3.95 (t, J = 6.4 Hz, 4 H), 6.51 (s, 1 H), 7.13 (s, 1 H); ^{13}C NMR (75 MHz, DMSO-d_6) δ 14.0, 22.1, 25.6, 28.6, 28.7, 28.8, 31.3, 40.8, 67.7, 97.1, 123.4, 127.8, 155.5.

3,6-Dibromopyromellitic Dianhydride (9). Preparation of this compound has been reported already,[22] but we describe here the revised procedures. A mixture of 3,6-dibromopyromellitic acid (9.89 g, 24 mmol), AcOH (90 g, 1.50 mol), and Ac_2O (5.00 g, 49 mmol) was heated at 140 °C for 3 h under a nitrogen atmosphere. The precipitate was collected by filtration, washed well with AcOH, and dried at 100 °C under vacuum, then purified by sublimation with Kugelrohr apparatus (280 °C/5 Pa) to give **9** in 57% yield (5.10 g, 13.6 mmol) as colorless needles: mp >300 °C; ^{13}C NMR (75 MHz, acetone-d_6) δ 117.4, 138.7, 159.0. Anal. Calcd for $C_{10}Br_2O_6$: C, 31.95. Found: C, 31.64.

[2 + 2] Tetrabromo-Substituted Pyromellitic Diimide-Based Macrocycle (10). A solution of the anhydride **9** (1.06 g, 2.71 mmol) in dry THF (180 mL) and a solution of the amine **8** (1.01 g, 2.71 mmol) in dry THF (180 mL) were simultaneously added to dry THF (50 mL) at 50 °C over a period of 4 h with stirring under a nitrogen atmosphere. After the addition, the reaction mixture was stirred at 50 °C for 24 h, and the reaction mixture was evaporated in vacuo to dryness to give the amic acid. A suspension of the amic acid and NaOAc (889 mg, 10.8 mmol) in Ac_2O (40 mL) was stirred at room temperature for 3 h under a nitrogen atmosphere, then heated at 100 °C for 1 h. The reaction mixture was poured into water, and the precipitate was collected by filtration. The precipitate was continuously extracted with CH_2Cl_2 in a Soxhlet extractor, and the extract was evaporated in vacuo to dryness. The residue was purified by silica gel column chromatography eluting with $CHCl_3$/AcOEt (50:1, v/v) and recrystallization from $CHCl_3$/hexane to give **10** in 12% yield (235 mg, 0.16 mmol) as a pale yellow powder: mp >300 °C; IR (KBr) ν_{max} 2925, 2856, 1772 ($\nu_{C=O}$), 1718 ($\nu_{C=O}$), 1621, 1594, 1513, 1436, 1392, 1307, 1193, 1114, 954 cm^{-1}; ^{1}H NMR (300 MHz, $CDCl_3$) δ 1.02 (t, J = 7.4 Hz, 12 H), 1.52−1.61 (m, 8 H), 1.86 (tt, J = 6.3 Hz, 8 H), 4.07 (t, J = 6.3 Hz, 8 H), 4.86 (s, 8 H), 6.49 (s, 2 H, ArH), 6.52 (s, 2 H); ^{13}C NMR (75 MHz, CD_2Cl_2) δ 13.7, 19.4, 35.5, 68.6, 97.0, 114.0, 115.7, 124.9, 135.9, 156.8, 163.0 (one signal of alkyl carbon overlaps with that of other ones); FAB-MS (NBA, positive) 1464 (M$^+$). Anal. Calcd for $C_{68}H_{80}Br_4N_4O_{12}$: C, 55.75; H, 5.50; N, 3.82. Found: C, 55.74; H, 5.47; N, 3.83.

***N,N′*-Di-*n*-butyl-3,6-dibromopyromellitic Diimide (11).** To a solution of the anhydride **9** (505 mg, 1.34 mmol) in dry THF (65 mL) was added a dry THF solution (5 mL) of butylamine (294 mg, 4.03 mmol) at room temperature under a nitrogen atmosphere. After the mixture was stirred for 12 h, the reaction mixture was evaporated in vacuo to dryness to give the amic acid. A suspension of the amic acid and NaOAc (439 mg, 5.36 mmol) in Ac_2O (20 mL) was heated at 100 °C for 1 h, the reaction mixture was poured into water, and the precipitate was collected by filtration. The precipitate was purified by silica gel column chromatography eluting with CH_2Cl_2 to give **11** in 73% yield (473 mg, 0.97 mmol) as a white powder: mp >300 °C; IR (KBr) ν_{max} 2959, 1767 ($\nu_{C=O}$), 1712 ($\nu_{C=O}$), 1439, 1401, 1364, 1351, 1339, 1181, 1169, 1070 cm^{-1}; ^{1}H NMR (300 MHz, $CDCl_3$) δ 0.96 (t, J = 7.4 Hz, 6 H), 1.38 (qt, J = 7.4 Hz, 4 H), 1.69 (tt, J = 7.4 Hz, 4 H), 3.74 (t, J = 7.4 Hz, 4 H); ^{13}C NMR (75 MHz, $CDCl_3$) δ 13.6, 20.0, 30.2, 38.8, 114.0, 136.2, 163.5; FAB-MS (NBA, positive) 486 (M$^+$). Anal. Calcd for $C_{18}H_{18}Br_2N_2O_4$: C, 44.47; H, 3.73; N, 5.76. Found: C, 44.54; H, 3.71; N, 5.75.

[2 + 2] Tetrabromo-Substituted Macrocycle (12). According to similar procedures reported for **10**, **12** was obtained in 12% yield from the anhydride **9** and 1,3-bis(aminomethyl)-4,6-di-*n*-butoxybenzene[17b,20] as a pale yellow powder: mp >300 °C; IR (KBr) ν_{max} 2958, 2871, 1772 ($\nu_{C=O}$), 1720 ($\nu_{C=O}$), 1621, 1595, 1513, 1437, 1388, 1307, 1193, 1114, 954 cm^{-1}; ^{1}H NMR (300 MHz, CD_2Cl_2) δ 1.02 (t, J = 7.4 Hz, 12 H), 1.52−1.61 (m, 8 H), 1.86 (tt, J = 6.3 Hz, 8 H), 4.07 (t, J = 6.3 Hz, 8 H), 4.86 (s, 8 H), 6.49 (s, 2 H), 6.52 (s, 2 H); ^{13}C NMR (75 MHz, CD_2Cl_2) δ 13.7, 19.4, 35.5, 68.6, 97.0, 114.0, 115.7, 124.9, 135.9, 156.8, 163.0; FAB-MS (NBA, positive) 1241 [(M + H)$^+$]. Anal. Calcd for $C_{52}H_{48}Br_4N_4O_{12}$: C, 50.34; H, 3.90; N, 4.52. Found: C, 50.40; H, 3.86; N, 4.57.

Preparation of Clathrate Crystals. Recrystallization of **3** (4 mg, 7.6 × 10^{-3} μmol) from the aniline solution (500 μL) at 15 °C gave yellow crystals on standing for 5 d. The CH_2Cl_2 solution (2 mL) of **3** (5 mg, 9.5 × 10^{-3} μmol) in the presence of *p*-dimethoxybenzene (19 mg, 1.4 × 10^{-1} μmol) was allowed to evaporate very slowly at 15 °C for 4 d to give yellow crystals. Recrystallization of **3** (4 mg, 7.6 × 10^{-3} μmol) from the $CHCl_3$ solution (2 mL) in the presence of α-naphthol (8 mg, 5.3 × 10^{-2} μmol) by vapor diffusion with hexane (4 mL) at room temperature gave yellow crystals on standing for 3 d. Recrystallization of **3** (4 mg, 7.6 × 10^{-3} μmol) from the $CHCl_3$ solution (2 mL) in the presence of indole (7 mg, 5.3 × 10^{-2} μmol) by vapor diffusion with hexane (4 mL) at room temperature gave yellow crystals on standing for 2 d.

Determination of Association Constants (K_{CT}). In the presence of a large amount of π-donors, K_{CT} values of the CT complexes were determined in $CHCl_3$ by a spectrophotometric procedure based on the Benesi−Hildebrand relationship[37] at 25 °C. In all cases, linear correlations were observed, indicating a 1:1 molar ratio for the CT complexes. From the linear plot of Δabsorbance against [π-donor]$^{-1}$, consisting of at least eight points, the slope was estimated as $(K_{CT}\epsilon_{CT})^{-1}$ and the intercept as $(\epsilon_{CT})^{-1}$. Linear fits obtained by the least-squares had a correlation coefficient of >0.999.

X-ray Crystallographic Structural Analysis. Data are summarized in the Supporting Information.

Theoretical Methods. All calculations were performed with the Gaussian 03[40] suite of programs. Optimized structure, frequency calculations, and single-point energy calculations were performed with the Becke's three-parameter hybrid functional (B3)[41] with the correlation functional of Lee, Yang, and Parr (LYP).[42,43] Restricted

(40) Frisch, M. J.; Trucks, G. W.; Schlegel, H. B.; Scuseria, G. E.; Robb, M. A.; Cheeseman, J. R.; Montgomery, J. A., Jr.; Vreven, T.; Kudin, K. N.; Burant, J. C.; Millam, J. M.; Iyengar, S. S.; Tomasi, J.; Barone, V.; Mennucci, B.; Cossi, M.; Scalmani, G.; Rega, N.; Petersson, G. A.; Nakatsuji, H.; Hada, M.; Ehara, M.; Toyota, K.; Fukuda, R.; Hasegawa, J.; Ishida, M.; Nakajima, T.; Honda, Y.; Kitao, O.; Nakai, H.; Klene, M.; Li, X.; Knox, J. E.; Hratchian, H. P.; Cross, J. B.; Bakken, V.; Adamo, C.; Jaramillo, J.; Gomperts, R.; Stratmann, R. E.; Yazyev, O.; Austin, A. J.; Cammi, R.; Pomelli, C.; Ochterski, J. W.; Ayala, P. Y.; Morokuma, K.; Voth, G. A.; Salvador, P.; Dannenberg, J. J.; Zakrzewski, V. G.; Dapprich, S.; Daniels, A. D.; Strain, M. C.; Farkas, O.; Malick, D. K.; Rabuck, A. D.; Raghavachari, K.; Foresman, J. B.; Ortiz, J. V.; Cui, Q.; Baboul, A. G.; Clifford, S.; Cioslowski, J.; Stefanov, B. B.; Liu, G.; Liashenko, A.; Piskorz, P.; Komaromi, I.; Martin, R. L.; Fox, D. J.; Keith, T.; Al-Laham, M. A.; Peng, C. Y.; Nanayakkara, A.; Challacombe, M.; Gill, P. M. W.; Johnson, B.; Chen, W.; Wong, M. W.; Gonzalez, C.; Pople, J. A. *Gaussian*03, revision C.02; Gaussian, Inc.: Wallingford, CT, 2004.

(41) Becke, A. D. *J. Chem. Phys.* **1993**, *98*, 5648–5652.

(42) Lee, C.; Yang, W.; Parr, R. G. *Phys. Rev. B* **1988**, *37*, 785–789.

calculations were performed, as all relevant species were closed shell molecules.

Acknowledgment. S.K. thanks the JSPS for a Research Fellowship for Young Scientists. This work was supported by a Theme Project (Prof. Tahsin J. Chow) from the Institute of Chemistry, Academia Sinica, Taiwan R.O.C., as well as a Grant-in-Aid for Scientific Research (B) (No. 18350025) and the Global COE program, "Science for Future Molecular Systems" from the Ministry of Education, Culture, Sports, Science and Technology of Japan. We are grateful to Professor Dr. Tsutomu Ishi-i (Kurume National College of Technology) for the fluorescence spectroscopic measurement.

Supporting Information Available: General experimental methods, ^{1}H and ^{13}C NMR spectra of **2**, **3**, **6**−**8**, **10**, **11**, and **12**, fluorescent properties of **1** and *N*,*N*′-di-*n*-butylpyromellitic diimide, complexation studies with **3** and π-donors, X-ray crystallographic structure analysis, MALDI-TOF-MS spectrum of **3**, concentration-dependent ^{1}H NMR spectra of **3**, and theoretical calculations of **2**, **2′**, and **3**. This material is available free of charge via the Internet at http://pubs.acs.org.

JO800283R

(43) Miehlich, B.; Savin, A.; Stoll, H.; Preuss, H. *Chem. Phys. Lett.* **1989**, *157*, 200–206.